THE JOURNAL OF PHYSICAL CHEMISTRY A

ARTICLE

pubs.acs.org/JPCA

Spectroscopy and Fragmentation of Undercoordinated Bromoiridates

Jesse C. Marcum,[†,‡] Anna I. Krylov,[§] and J. Mathias Weber*[,†]

[†]JILA, NIST, and Department of Chemistry and Biochemistry, University of Colorado, Boulder, Colorado 80309, United States

[§]Department of Chemistry, University of Southern California, Los Angeles, California 90089-0482, United States

ABSTRACT: We report gas-phase electronic photodissociation spectra of the undercoordinated bromoiridate complexes $IrBr_4^-$ and $IrBr_5^-$ at photon energies from 1 to 5.6 eV. Both ions have open-shell ground states with low-symmetry structures. The fragmentation is characterized by thresholds for the loss of one Br atom for $IrBr_4^-$ and one or two Br atoms for $IrBr_5^-$. The experimental spectra consist of ligand-to-metal charge transfer transitions and reveal a large density of electronic states that can be recovered by time-dependent density functional theory.

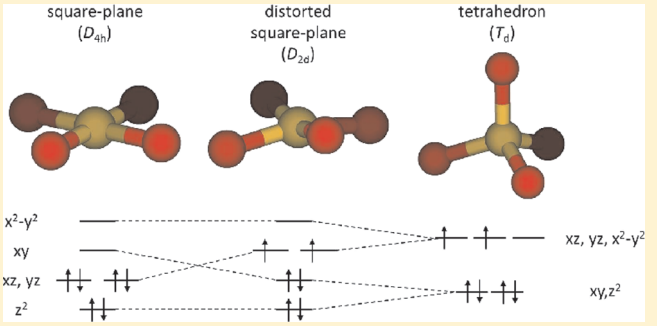

INTRODUCTION

The last two decades have seen a resurgence of physical and chemical experiments on transition metal complexes, in part due to the advent of experimental techniques that allow for the study of such complexes in the gas phase.[1−11] Studies of transition metal complexes in the gas phase are advantageous because they can provide detailed information on *intrinsic* molecular properties by isolating species of interest from the perturbing effects of solvent or counterions. Although many studies have been performed on fully coordinated transition metal complexes,[1−11] much less information is available on smaller, undercoordinated species. Despite this lack of attention, it would be advantageous to develop an understanding of these species because they are likely to play important roles in transition metal chemistry. For instance, many transition metal complexes readily participate in ligand exchange reactions. In cases where exchange occurs via a dissociative mechanism, undercoordinated species will exist as transient, reactive intermediates.[12,13] Additionally, such undercoordinated, reactive species may be formed following photodissociation as a consequence of the light sensitivity of many transition metal complexes. Obtaining relevant thermodynamic and spectroscopic data on these species in situ is nontrivial due to their transient nature. Furthermore, undercoordinated complexes are likely to be present as part of a complicated mixture, where overlapping spectral signatures from a large number of related species complicate analysis. Gas-phase studies on mass-selected species can be used to circumvent these problems by probing the complexes as individual, isolated species.

In addition to their potential importance in solution-phase processes, undercoordinated species are also of interest for more fundamental processes in the gas phase. In particular, many experiments have been performed to probe the nature of the repulsive Coulomb barriers (RCBs) that exist in multiply charged anionic compounds.[1−11,14−18] The specific details of a RCB are dependent upon a number of factors that include the asymptotic behavior of multiply charged anions as dissociation occurs. Upon dissociation, each electronic state of the products will correspond to a unique RCB on the potential energy surface.[1,14,15,19,20] However, information on the electronic excited states of fragment species that contain the transition metal is scarce. Many of these species correspond to undercoordinated transition-metal complexes. Therefore, determining their thermodynamic and spectroscopic properties would be desirable.

This paper describes the fragmentation and electronic photodissociation spectroscopy of two undercoordinated bromoiridates, $IrBr_5^-$ and $IrBr_4^-$. Both species are well-known fragments of the prototypical gas-phase multiply charged anion $IrBr_6^{2-}$[6,7,10,11,17] and have been observed following collision-induced-dissociation[7,10,17] as well as photodissociation.[6,11,21] The ion $IrBr_5^-$ corresponds to the lowest-energy decay pathway of $IrBr_6^{2-}$, where it is formed via ionic fragmentation and is accompanied by formation of Br^- fragment ions.[6,7,10,11,17,21] The ion $IrBr_4^-$ can be formed from decay of $IrBr_6^{2-}$ via a number of possible mechanisms including thermal dissociation, direct dissociation on a repulsive curve, and dissociative electron detachment.[6,7,10,11,17,21] In particular, it has been observed as a decay product of $IrBr_6^{2-}$ following a two-photon process.[6,11,21] However, at photon energies in the visible region of the spectrum, it was not clear whether $IrBr_4^-$ is formed as a primary photoproduct following absorption of two photons by $IrBr_6^{2-}$ or as a secondary photoproduct whereby the first photon promotes dissociation of $IrBr_6^{2-}$ into the primary photoproduct, $IrBr_5^-$, which dissociates upon absorption of the second photon.[6,11] For the latter process to occur, $IrBr_5^-$ would have to absorb at some of the same wavelengths as $IrBr_6^{2-}$ and have a low-enough dissociation threshold to facilitate breaking of an Ir−Br bond.

Received: September 15, 2011
Revised: October 10, 2011
Published: October 12, 2011

In this paper, experimental photofragment action spectra for the parent ions $IrBr_4^-$ and $IrBr_5^-$ are presented and discussed in the context of a molecular orbital analysis, calculated electronic spectra and fragmentation threshold energies.

METHODS

Instrumental Setup. The experimental apparatus has been described in detail elsewhere.[22] Briefly, it consists of an electrospray ionization (ESI) source coupled to a reflectron time-of-flight mass spectrometer (RETOF) and a UV−vis optical parametric converter. Ions of interest were produced using electrospray ionization of an ∼4 mM aqueous solution of K_2IrBr_6 (Sigma-Aldrich). Following accumulation in a hexapole ion trap, the ions are injected into the acceleration region of a Wiley−McLaren RETOF. At the first space focus of the RETOF ions of interest are mass selected using a pulsed mass gate and irradiated with the output of a tunable optical parametric converter (220−2500 nm). Fragment ions are separated from any remaining undissociated parent ions and mass-analyzed using a two-stage reflectron prior to detection on a dual microchannel plate detector in the second space focus of the mass spectrometer. By monitoring the fragment ions as a function of photon energy, we were able to obtain photodissociation action spectra. All spectra are corrected for laser fluence as well as for unimolecular decay of metastable parent ions. The $IrBr_5^-$ and $IrBr_4^-$ ions that were studied in this experiment are presumably formed by fragmentation of $IrBr_6^{2-}$ in the initial stages of our ESI source prior to reaching the room-temperature hexapole trap where ions are assumed to reach thermal equilibrium.

Computational Details. To determine theoretical thresholds for fragmentation channels, geometry optimizations were performed on the parent as well as fragment ions using the TURBOMOLE V6.2 suite of programs.[23] We employed density functional theory (DFT)[24] with the B3LYP functional[25,26] and a def2-TZVPP basis set[27] for all atoms. The def2-ecp effective core potential (multielectron fit to Wood−Boring orbital energies)[28] was used to account for scalar relativistic effects. All geometry optimizations were performed without symmetry constraints starting from several initial structures that are typical of transition metal complexes for coordination numbers of the species studied in this experiment. For example, optimizations for four-coordinate species were started from square-planar, tetrahedral, and butterfly geometries and five-coordinate species were started from square-pyramidal and trigonal-bipyramidal geometries. Additionally, optimizations were performed for a variety of unrestricted, open-shell multiplicities. Vibrational frequencies were calculated using analytical second derivatives.[29,30] The obtained frequencies were used to correct the calculated gas-phase thresholds for zero-point energy. For comparison to apparent experimental thresholds, the vibrational energy content of the ions was taken into account using the equation

$$U_{vib} = \sum_i \frac{h\nu_i}{(e^{h\nu_i/kT} - 1)}$$

where ν_i represents the frequencies of the individual vibrational modes, h is Planck's constant, k is the Boltzmann constant, and T is the temperature of the ions. Because ions are accumulated in a room-temperature hexapole ion trap we assume the ion temperature to be 300 K.

Electronic spectra of $IrBr_4^-$ and $IrBr_5^-$ were characterized by time-dependent DFT (TDDFT),[31,32] spin-flip DFT (SF-DFT)[33] and equation-of-motion (EOM)[34,35] methods using the QChem suite of programs.[36] The PBE0 functional[37] was employed and the LANL2DZ basis set[38] including its effective core potential (ECP) was used for all atoms.

The TDDFT calculations were validated by comparison with EOM-EE-CCSD[35] (EOM coupled-cluster with single and double substitutions for excitation energies) using the same ECP and basis set. For the 10 lowest states of $IrBr_5^-$, the character (i.e., oscillator strength and leading excitation amplitudes) and excitation energies predicted by TDDFT and EOM agree well. The EOM excitation energies are consistently higher by 0.12−0.19 eV. A larger basis set, of a triple-ζ quality, CRENBL,[39,40] was also tested for the 10 lowest states. The changes in excitation energies due to the basis set increase did not exceed 0.05 eV.

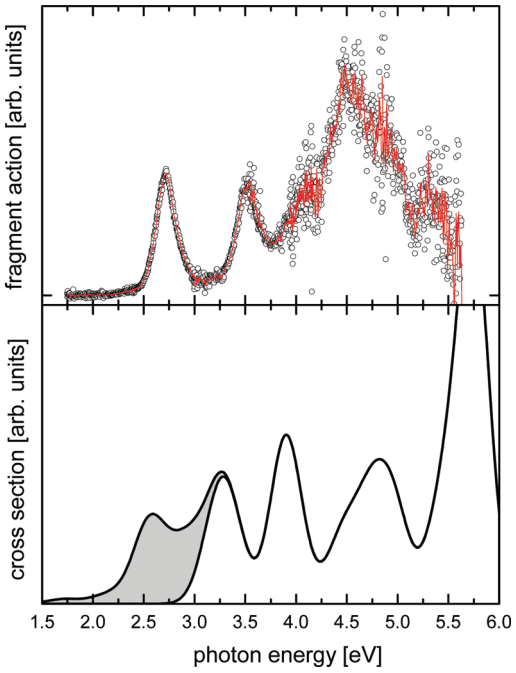

Figure 1. Photodissociation action spectrum of $IrBr_4^-$ obtained by monitoring $IrBr_3^-$ fragments (top) as a function of photon energy, compared to the calculated absorption cross section (bottom). Observation of the transitions in the shaded area of the calculated spectrum is likely to be energetically inaccessible in the experiment (see text), resulting in an absorption spectrum similar to that for the nonshaded curve. On the basis of the peak shifts (0.5 eV) of the calculated bands compared to the experimental bands, the nonshaded spectrum was generated by including only states 0.5 eV above the experimentally observed onset of the spectrum. All excited states found in the calculations are convolved with Gaussians with 0.3 eV width.

RESULTS AND DISCUSSION

Photodissociation Spectra and Ionic Fragment Channels for $IrBr_4^-$. Following irradiation of $IrBr_4^-$, the two fragment ions observed were Br^- and $IrBr_3^-$, the latter corresponding to the loss of a neutral bromine atom. Of the two observed fragment channels, $IrBr_3^-$ yielded substantially higher fragment ion intensities. The Br^- fragment ion intensity was so low that it prevented us from using this fragment channel to obtain a photodissociation spectrum or to quantify the branching ratios. This may be due to the low kinetic energy of Br^- ions following dissociation, resulting in correspondingly low detection efficiencies.

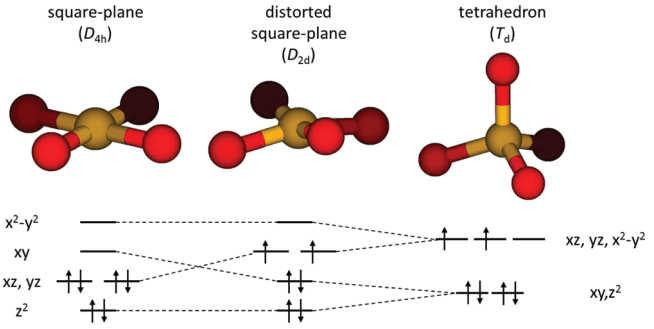

Figure 2. Several potential geometries of the $IrBr_4^-$ complex with their corresponding schematic molecular orbital energy diagrams. Note that the relative energies in each molecular orbital diagram are not to scale. The middle structure, corresponding to a distorted square-plane with D_{2d} symmetry, is calculated to be the lowest energy geometry when it has a triplet electron configuration.

A photodissociation spectrum of $IrBr_4^-$, obtained by monitoring $IrBr_3^-$ ions as a function of photon energy, is shown in Figure 1. The spectrum consists of three main features; a peak centered near 2.7 eV, a second peak centered near 3.5 eV and a broad feature centered near 4.5 eV that has apparent high- and low-energy shoulders around 4.1 and 5.3 eV, respectively.

To interpret $IrBr_4^-$ spectral features, it is necessary to understand the primary elements of the electronic structure of the complex. A full description of the electronic structure of these complexes is a tremendous undertaking due to a number of complex factors that include spin−orbit coupling, relativistic effects, and high density of electronic states as well as multiple open-shell configurations. However, much insight can already be gained by use of a simple, qualitative molecular orbital approach to predict the initial and final electron configurations of the complex. The ground-state structure of the complex predicted by B3LYP calculations lies between a square-plane and a tetrahedron and has a triplet configuration (Figure 2). This structure and configuration are approximately 220 meV lower in energy (adiabatically) than a square-planar triplet and approximately 460 meV lower in energy than a square-planar singlet. This result can be understood using a molecular orbital picture that consists of four-coordinate Ir(III) in a d^6 electron configuration with contributions from ligand p-orbital donors. Structures consisting of a tetrahedron (T_d symmetry) and square-plane (D_{4h} symmetry) constitute high-symmetry limits to the possible geometries of $IrBr_4^-$ with well-known molecular orbital diagrams.[13,41,42] These geometries, along with their corresponding molecular orbital diagrams, are shown in Figure 2. For $IrBr_4^-$ to have a tetrahedral geometry, four electrons will need to be distributed in the upper t_2 state. This configuration should induce Jahn−Teller distortion to lower symmetry. The most direct way of lowering the symmetry is for the four bromide ligands to move toward being square-planar so that the molecule has D_{2d} symmetry. At the opposite extreme, all four ligands and the iridium atom lie in the same plane so that $IrBr_4^-$ adopts a square-planar geometry. In this geometry, the energy gap between the d(xy) and doubly degenerate d(xz) and d(yz) orbitals should be small enough to open up the possibility of both high- and low-spin configurations. If the complex adopts a low-spin singlet configuration, then a square-planar geometry will be the most stable configuration and distortion should not occur. However, if it adopts a high-spin configuration, Jahn−Teller distortion to lower symmetries is expected. In this case, the bromide ligands should move out of the plane toward a tetrahedron, resulting in the complex having D_{2d} symmetry. This distortion will lead to a change in the molecular orbital energies so that the configuration has two paired electrons in the d(xy) orbital and two unpaired electrons distributed among the two doubly degenerate d(xz) and d(yz) orbitals. The B3LYP results are in good agreement with the molecular orbital picture developed from both extremes. In either case, this lowering of the molecular symmetry to D_{2d} has significant consequences for the interpretation of spectral features. Because the DFT-predicted structure lies closer to a square-planar structure than a tetrahedron (Figure 2), it is easier to approach the spectroscopy from this limit.

In the square-planar, high-symmetry (D_{4h}) limit, ligand-to-metal charge-transfer (LMCT) bands would be expected to dominate the electronic spectra of $IrBr_4^-$. These transitions promote electron density from predominantly ligand-based molecular orbitals to metal-based d-orbitals. Lower-energy transitions would involve promoting electron density into the doubly degenerate d(xz) and d(yz) metal orbitals (e_g in the D_{4h} point group) and higher-energy transitions to the d(x^2-y^2) orbital (b_{1g} in the D_{4h} point group). In principle, d−d transitions should be in the same approximate energy range as the LMCT bands but are electric-dipole forbidden and should be of considerably weaker intensity. However, the situation changes considerably when the geometry distorts to the lower-symmetry D_{2d} point group. When this occurs, the number of irreducible representations is greatly reduced, allowing metal d-orbitals to mix with various ligand orbitals that would not transform together in the D_{4h} point group. Consequently, the allowed transitions cannot be described as of "purely" LMCT character but will also include character due to d−d transitions. Additionally, this mixing will result in a splitting of the ligand orbitals involved in the transitions, greatly increasing the number of bands to be expected in the spectrum. Whereas detailed spectral assignments are beyond the simple molecular orbital arguments outlined above, the analysis of the TDDFT states reveals excited states with a complicated mixed character, where the observed features (i.e., oscillator strength) correspond to transitions that involve promoting electron density from mixed ligand−metal orbitals into either the metal-based d(x^2-y^2) or doubly degenerate d(xz) and d(yz) orbitals.

In addition to the factors mentioned above, it is also necessary to consider the thresholds for each fragment channel because photodissociation can only occur if enough energy is deposited into the molecule during absorption. Theoretical threshold energies for $IrBr_4^-$ were obtained using B3LYP calculations and are summarized in Table 1. The two lowest energy fragment channels correspond to loss of either a neutral bromine atom or a Br^- ion, and both have thresholds of approximately 2.7 eV. When compared to the $IrBr_4^-$ photodissociation action spectrum, the threshold for $IrBr_3^-$ is found to correspond roughly to the first peak in the spectrum. In principle, $IrBr_3^-$ should not be formed at photon energies less than the appropriate dissociation threshold. However, parent ions are assumed to reach thermal equilibrium in the room temperature hexapole ion trap, and they should have vibrational energies corresponding to a temperature of approximately 300 K prior to irradiation. On the basis of calculated harmonic frequencies, this temperature corresponds to an average vibrational energy of approximately 0.16 eV. If an additional 1.5 kT of rotational energy is included, there will be a total internal energy of approximately 0.2 eV. Taking this internal energy into account suggests that we should begin to see $IrBr_3^-$ fragment ions at approximately 2.5 eV, which is in good agreement with the onset of the features in our spectrum. This also suggests that any spectral

Table 1. Calculated Threshold Energies (B3LYP) for Various Fragment Channels Resulting from the Photodissociation of $IrBr_4^-$ [a]

fragment channel	energy (eV)
$IrBr_3^0 + Br^0 + e^-$	5.97
$IrBr_2^- + 2Br^0$	5.16
$IrBr_2^0 + Br^- + Br^0$	4.76
$IrBr_4^0 + e^-$	4.11
$IrBr_3^0 + Br^-$	2.71
$IrBr_3^- + Br^0$	**2.70**

[a] The channel corresponding to experimentally observed fragments is in bold.

features present below ~2.5 eV should not be observed because absorption of a photon does not provide enough energy for fragmentation.

Other product channels that have calculated thresholds within the energy range of the current experiment correspond to electron detachment from $IrBr_4^-$ at 4.1 eV and loss of two neutral bromine atoms to form $IrBr_2^-$ at 5.16 eV. However, we do not observe $IrBr_2^-$ fragments and our experiment does not have the ability to detect electrons or to selectively identify neutral fragments.

The multiplicity of the ground state obtained by B3LYP calculations as discussed above was validated by SF-DFT, which is capable of describing multiconfigurational open-shell wave functions (e.g., diradicals). The lowest states of $IrBr_4^-$ were computed by SF-DFT from a high-spin triplet reference state. The singlet state was found to be 0.49 eV above the triplet state (vertically), and the singlet state has closed-shell character (leading configuration weight of 0.9). Thus, it can be well described by regular DFT. The spectrum of $IrBr_4^-$ was generated using 58 TDDFT states computed from the high-spin triplet reference state, showing a very large density of states in the spectral window of the experiment.

A priori, the agreement of experimental and calculated spectra (Figure 1) for $IrBr_4^-$ is expected to be relatively poor, because TDDFT does not have quite sufficient configurational flexibility to describe excited states from the triplet reference state. The calculations show mainly four broad, congested bands for energies up to 5 eV, each consisting of several electronic transitions. Because the calculated threshold energy for the observed fragment channel is in the region of the lowest of these bands (Table 1), fragmentation is likely to be energetically inaccessible upon excitation in this energy range. The remaining calculated bands are ca. 0.5 eV too high in energy, but the overall shape of the spectrum is compatible with the experimental spectrum (Figure 1). All bright states seem to be dominated by ligand-to-metal transitions.

Photodissociation Spectra and Ionic Fragment Channels for $IrBr_5^-$. Following irradiation of $IrBr_5^-$, the two fragment ions observed are $IrBr_4^-$ and $IrBr_3^-$, corresponding to the loss of one and two neutral bromine atoms, respectively. A search was conducted for Br^- fragment ions but none were found.

Photodissociation spectra for $IrBr_5^-$ obtained by monitoring $IrBr_4^-$ and $IrBr_3^-$ fragment ions are shown in Figure 3. The action spectrum for the $IrBr_4^-$ fragment channel consists of four main peaks centered near 1.75, 2.05, 3.2, and 4.15 eV as well as a plateau between 2.25 and 2.8 eV. Following the peak at 4.15 eV, the ion signal decreases to zero and does not return at higher photon energies accessible in our experiment. The spectrum obtained by monitoring the $IrBr_3^-$ fragment channel is entirely different. This spectrum only shows an onset and rise of fragment

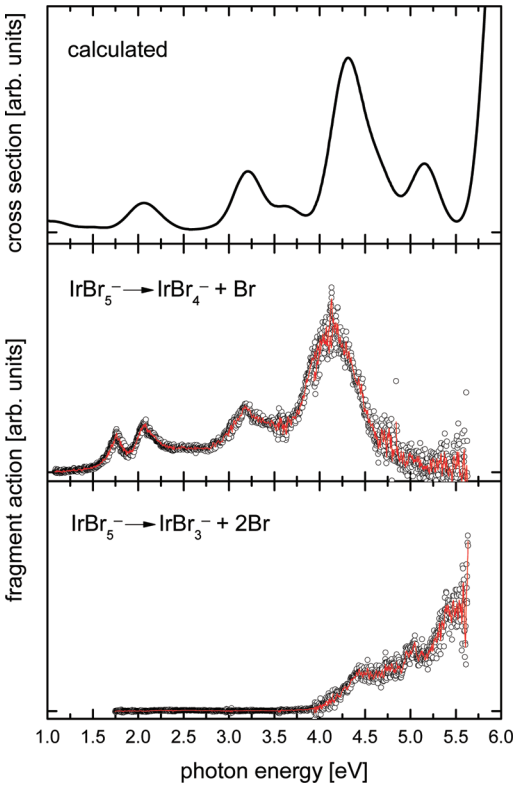

Figure 3. Calculated absorption cross section (top) compared to experimental photodissociation action spectra of $IrBr_5^-$ obtained by monitoring $IrBr_4^-$ (center) and $IrBr_3^-$ (bottom) fragment ions as a function of photon energy. The calculated excited states are convolved with Gaussians with 0.3 eV width.

ion signal beginning near 4.0 eV that has several shoulders. Additionally, there are several very minor features between 2.1 and 3.5 eV.

As in the case of $IrBr_4^-$, several important insights can be made by considering a qualitative molecular orbital picture for $IrBr_5^-$. The lowest energy structure for $IrBr_5^-$ is shown in Figure 4 and consists of a distorted square-based pyramid of doublet multiplicity. The ground-state multiplicity of $IrBr_5^-$ was validated by SF-DFT and EOM-SF calculations using a quartet reference state,[35] confirming that the ground state is indeed a doublet with a quartet state about 0.4−0.5 eV higher in energy. The observed distortions are most easily understood by considering the d^5 configuration of the complex. For simplicity, only σ-bonds are included at first and π-bonds are accounted for as a final consideration. Using this approach, the initial geometry that is considered has the iridium atom slightly above the plane consisting of the four equatorial bromide ligands with the final, axial ligand above the iridium. This geometry, along with its metal-based molecular orbital diagram, is shown in Figure 4. The lowest of the d-block orbitals consists of a d(xy) orbital, followed by a doubly degenerate level made up of the d(xz) and d(yz) orbitals and the d(z^2) and eventually the d(x^2-y^2) orbitals at higher energies. Because of the d^5 configuration, the doubly degenerate level will be the highest-occupied molecular orbital (HOMO) but will lead to fractional occupation numbers. This will cause the molecule to distort by increasing the bond angles between the axial Ir−Br bond and one of the two pairs of opposing equatorial Ir−Br ligand bonds so that the d(xz) and d(yz) orbitals split

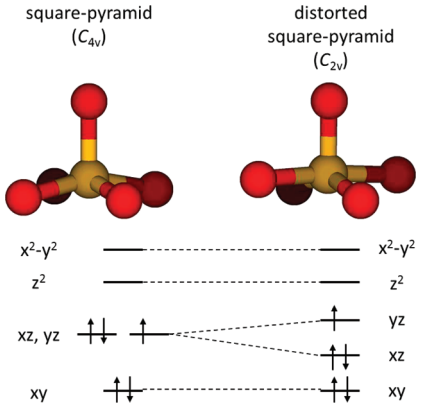

Figure 4. Two potential geometries of the $IrBr_5^-$ complex with their corresponding schematic molecular orbital energy diagrams. Note that the relative energies in each molecular orbital diagram are not to scale. The structure on the right, corresponding to a distorted square-pyramid with C_{2v} symmetry, is calculated to be the lowest energy geometry and has a doublet configuration.

(Figure 4). Up until this point, ligand p-orbitals have not been considered. In principle, they should not provide a significant problem for analysis because they will simply cause a slight reordering of all metal-based molecular orbitals. However, the expected distortion of $IrBr_5^-$ will result in the molecule having C_{2v} symmetry, leading to a substantial degree of mixing between many of the molecular orbitals that would belong to different irreducible representations in a higher-symmetry point group. As in the case of $IrBr_4^-$, this will preclude assignments of transitions to purely LMCT or metal d−d character. However, the two remaining d-block orbitals, d(z^2) and d(x^2-y^2), are not expected to exhibit as much π-mixing with ligand p-orbitals as the d(xy), d(xz), and d(yz) orbitals. This means that the observed spectral features should still involve transitions that promote electron density into these orbitals (in addition to the singly occupied HOMO), similar to the transitions observed for the octahedral complex $IrBr_6^{2-}$.[6,21] The main distinction would be the complexity of the low-lying orbitals involved in the $IrBr_5^-$ transitions.

The calculations reveal a very high density of electronic states with 71 TDDFT states in the energy range from 0.33 to 7.22 eV. The spectrum shown in Figure 3 was computed convolving these states with Gaussians. The split between the experimentally observed bands at 1.75 and 2.05 eV is not recovered by the calculations, and the higher lying calculated bands are too high by up to 0.2 eV, but the overall agreement between the calculated and experimental spectrum for the $IrBr_4^-$ fragment channel is remarkable, given the complexity of the electronic states. All bright states appear to be dominated by ligand-to-metal transitions. The good agreement between the calculated absorption cross section and the experimental action spectrum for the $IrBr_4^-$ fragment channel clearly demonstrates that the observed bands and their intensities are dominated by purely electronic factors, i.e., the density of electronic excited states and their oscillator strengths, whereas broadening due to vibrational structure is not resolvable due to multiple overlapping electronic transitions.

To understand why the action spectra associated with the $IrBr_4^-$ and $IrBr_3^-$ fragment channels are so different, we calculated the threshold energies for each fragment channel. These values are summarized in Table 2. The threshold energy

Table 2. Calculated Threshold Energies (B3LYP) for Various Fragment Channels Resulting from the Photodissociation of $IrBr_5^-$ [a]

fragment channel	energy (eV)
$IrBr_4^0 + Br^0 + e^-$	5.57
$IrBr_5^0 + e^-$	4.52
$IrBr_3^0 + Br^- + Br^0$	4.17
$IrBr_3^- + 2Br^0$	**4.16**
$IrBr_4^0 + Br^-$	2.31
$IrBr_4^- + Br^0$	**1.46**

[a] Channels corresponding to experimentally observed fragments are in bold.

for the $IrBr_4^-$ fragment channel, corresponding to the loss of a single, neutral bromine atom, is calculated to be 1.46 eV and below the onset of spectral features in the corresponding action spectrum. Assuming that fragment ions have a temperature of about 300 K, they should have a vibrational energy of approximately 0.22 eV and, with 1.5 kT of rotational energy, an internal energy of approximately 0.26 eV. This means that fragment ions should not be energetically accessible below ∼1.2 eV. The second energetically accessible fragment channel corresponds to the loss of a single Br^- ion and has a calculated threshold at 2.3 eV. However, no Br^- fragment ions were detected, possibly due to their low detection efficiency.

The calculated threshold energy for the $IrBr_3^-$ channel, which corresponds to the loss of two neutral bromine atoms, is at 4.16 eV. This threshold value can be used to explain the drastic difference between the two action spectra obtained. In the vicinity of this threshold, the $IrBr_4^-$ channel dies out while the $IrBr_3^-$ channel grows in. At energies below the threshold, $IrBr_4^-$ should be the only energetically accessible fragment channel. Once this threshold is reached, loss of a second bromine atom becomes energetically possible, leading to the formation of $IrBr_3^-$. The fact that this switch in the active fragmentation channel occurs at energies slightly below the calculated threshold can be attributed to the roughly 0.26 eV of internal energy that the parent $IrBr_5^-$ ions should have prior to irradiation (assuming a parent ion temperature of 300 K). The decrease and ultimate disappearance of $IrBr_4^-$ fragment ion signal above this threshold can be explained by it having a reduced survival probability on the time scale of our experiment. If only a single bromine atom is lost at energies above this threshold, the produced $IrBr_4^-$ fragments should have a sufficient amount of energy remaining for further loss of a second bromine atom. Previous work by Rensing et al. on the fully coordinated species $IrBr_6^{2-}$ determined that certain electronic excitations will lead to dissociation on a time scale of ∼79 ps.[11] If dissociation of $IrBr_5^-$ (including loss of a second bromine atom) proceeds by means of a similar mechanism, fragmentation can be expected to occur on a much faster time scale than the ∼20 μs between irradiation and product ion mass analysis in our experiment. A similar energy dependence in the UV photodissociation of $AuCl_4^-$ has also been observed in recent work.[43]

Consideration of the threshold for $IrBr_3^-$ formation also raises the question as to what the minor features are that appear between 3.1 and 3.5 eV in the $IrBr_3^-$ action spectrum because there is only enough energy for the loss of a single bromine atom at these energies. These features can be explained on the basis of two-photon effects. If two photons are absorbed by the $IrBr_5^-$ fragment prior to dissociation, then there will be enough energy

available for loss of two bromine atoms. Alternatively, absorption of the first photon leads to dissociation of $IrBr_5^-$ into $IrBr_4^-$ which can then absorb a second photon and dissociate to form $IrBr_3^-$ product ions. Both of these pathways are possible because both $IrBr_5^-$ and $IrBr_4^-$ have absorption features in this region of the spectrum (see above). Similar behavior has previously been observed for the related system $IrBr_6^{2-}$, where loss of multiple ligands was interpreted as a two-photon process.[6] Regardless of the actual mechanism, features due to the absorption of two photons should be much less intense than features arising from single photon processes. The low fragment ion intensity supports this explanation, but prevented fluence measurements.

Very close to the threshold for the loss of two neutral bromine atoms is the threshold corresponding to concomitant loss of a neutral bromine atom and a Br^- ion (4.17 eV). However, this channel was not observed. Three additional dissociation channels are calculated to be energetically accessible within our spectral range. The first corresponds to electron detachment from $IrBr_5^-$ (4.52 eV), the second to dissociative detachment of $IrBr_5^-$ leading to the fragments $IrBr_4^0$ and a neutral bromine atom (5.57 eV), and the third to the loss of Br_2 (2.16 eV). Although these channels are energetically accessible, the photofragment action spectra do not show any discernible decrease of the dominant fragment channels at these energies.

Photoinduced Dissociation Mechanism. An important question to ask at this point concerns the mechanism by which bromoiridate dissociation occurs. At low energies, there is only enough energy available for $IrBr_5^-$ fragmentation to occur via loss of a single ligand. As soon as the loss of a second ligand becomes energetically accessible, this new channel turns on at the expense of the channel where only a single ligand is lost. The fact that this switching of the two channels occurs in the vicinity of the calculated fragmentation threshold suggests a thermal dissociation mechanism. This complementarity was not observed for the $IrBr_4^-$ ion. However, this is most likely due to the fact that the relevant threshold for loss of two ligands is calculated to be extremely close to the high-energy limit of our spectral range. Furthermore, no spectral features occur below the calculated threshold energy for loss of a single ligand. As $IrBr_4^-$ can be expected to behave similarly whether it is a parent ion or a hot intermediate ion formed during dissociation of $IrBr_5^-$, the behavior of $IrBr_4^-$ is consistent with fragmentation *via* a thermal mechanism.

SUMMARY AND CONCLUSIONS

We have identified prominent fragment channels and obtained photodissociation spectra for the undercoordinated bromoiridate complexes $IrBr_5^-$ and $IrBr_4^-$. The fragment action spectra for the $IrBr_5^-$ parent ion are found to be highly energy dependent. Complementarity in the two fragment channels, combined with DFT-calculated threshold energies, implies a thermal fragmentation mechanism. Similar mechanisms are expected for the $IrBr_4^-$ parent ion because the onset of spectral features coincides with the calculated threshold for the lowest-energy fragment channel.

Features observed in the $IrBr_5^-$ and $IrBr_4^-$ photodissociation spectra are complicated due to factors such as spin−orbit coupling, relativistic effects, as well as a large density of electronic states including multiple open-shell configurations. The latter cause geometric distortions that decrease their molecular symmetry to low-order point groups. This leads to significant mixing of ligand- and metal-based molecular orbitals and the respective electronic states, making assignment of spectral features impossible. The oscillator strength of the observed transitions are carried by LMCT-type excitations, which promote electron density to the metal-based $d(z^2)$ and $d(x^2-y^2)$ orbitals for $IrBr_5^-$ and to the metal-based $d(x^2-y^2)$ or doubly degenerate $d(xz)$ and $d(yz)$ orbitals for $IrBr_4^-$. The spectra can be described by TDDFT calculations that recover the large density of electronically excited states and suggest that the experimentally observed bands are dominated by electronic factors.

AUTHOR INFORMATION

Corresponding Author

*E-mail: weberjm@jila.colorado.edu.

Present Addresses

‡Department of Chemistry and Physics, Simmons College, Boston, MA 02115, U.S.A.

ACKNOWLEDGMENT

We thank Robert Warner, Dr. Ksenia Bravaya, and Dr. Kadir Diri for technical assistance. J.M.W. gratefully acknowledges the National Science Foundation (NSF) for funding through the JILA Atomic, Molecular and Optical Physics Frontier Center (Grant No. PHY-0551010) and through Grant No. CHE-0845618. We acknowledge the resources of the iOpenShell Center (http://iopenshell.usc.edu) supported by the NSF through the CRIF:CRF CHE-0625419 + 0624602 + 0625237 grant. A.I.K. also acknowledges the JILA Visiting Fellows Program and NSF support through the CHE-0951634 grant.

REFERENCES

(1) Wang, L. S.; Ding, C. F.; Wang, X. B.; Nicholas, J. B.; Nicholas, B. *Phys. Rev. Lett.* **1998**, *81*, 2667.
(2) Wang, X. B.; Ding, C. F.; Wang, L. S. *Phys. Rev. Lett.* **1998**, *81*, 3351.
(3) Wang, L. S.; Ding, C. F.; Wang, X. B.; Barlow, S. E. *Rev. Sci. Instrum.* **1999**, *70*, 1957.
(4) Wang, X. B.; Wang, L. S. *Phys. Rev. Lett.* **1999**, *83*, 3402.
(5) Bojesen, G.; Hvelplund, P.; Jorgensen, T. J. D.; Nielsen, S. B. *J. Chem. Phys.* **2000**, *113*, 6608.
(6) Friedrich, J.; Gilb, S.; Ehrler, O. T.; Behrendt, A.; Kappes, M. M. *J. Chem. Phys.* **2002**, *117*, 2635.
(7) Boxford, W. E.; El Ghazaly, M. O. A.; Dessent, C. E. H.; Nielsen, S. B. *Int. J. Mass Spectrom.* **2005**, *244*, 60.
(8) Löffler, D.; Weber, J. M.; Kappes, M. M. *J. Chem. Phys.* **2005**, *123*, 8585.
(9) Boxford, W. E.; Dessent, C. E. H. *J. Phys. Chem. A* **2005**, *109*, 5836.
(10) Burke, R. M.; Boxford, W. E.; Panja, S.; Nielsen, S. B.; Dessent, C. E. H. *Chem. Phys. Lett.* **2007**, *442*, 201.
(11) Rensing, C.; Ehrler, O. T.; Yang, J.; Unterreiner, A.; Kappes, M. M. *J. Chem. Phys.* **2009**, *130*, 234306.
(12) Langford, C. H.; Gray, H. B., *Ligand Substitution Processes*; W. A. Benjamin, Inc.: New York, 1966.
(13) Miessler, G. L.; Tarr, D. A. *Inorganic Chemistry*; 2nd ed.; Prentice-Hall; Upper Saddle River, NJ, 1998.
(14) Scheller, M. K.; Compton, R. N.; Cederbaum, L. S. *Science* **1995**, *270*, 1160.
(15) Dreuw, A.; Cederbaum, L. S. *Phys. Rev. A* **2001**, *63*, 049904.
(16) Dreuw, A.; Cederbaum, L. S. *Chem. Rev.* **2002**, *102*, 181.
(17) Boxford, W. E.; Pearce, J. K.; Dessent, C. E. H. *Chem. Phys. Lett.* **2004**, *399*, 465.

(18) Simons, J. *J. Phys. Chem. A* **2008**, *112*, 6401.
(19) Wang, X. B.; Wang, L. S. *J. Chem. Phys.* **1999**, *111*, 4497.
(20) Wang, X. B.; Nicholas, J. B.; Wang, L. S. *J. Chem. Phys.* **2000**, *113*, 653.
(21) Marcum, J. C.; Weber, J. M. *J. Chem. Phys.* **2009**, *131*, 194309.
(22) Marcum, J. C.; Halevi, A.; Weber, J. M. *Phys. Chem. Chem. Phys.* **1740**, *11*, 2009.
(23) Ahlrichs, R.; Bär, M.; Häser, M.; Horn, H.; Kölmel, C. *Chem. Phys. Lett.* **1989**, *162*, 165.
(24) Parr, R. G.; Yang, W., *Density-Functional Theory of Atoms and Molecules*; Oxford University Press: New York, 1989.
(25) Becke, A. D. *Phys. Rev. A* **1988**, *38*, 3098.
(26) Lee, C. T.; Yang, W. T.; Parr, R. G. *Phys. Rev. B* **1988**, *37*, 785.
(27) Weigend, F.; Häser, M.; Patzelt, H.; Ahlrichs, R. *Chem. Phys. Lett.* **1998**, *294*, 143.
(28) Andrae, D.; Haussermann, U.; Dolg, M.; Stoll, H.; Preuss, H. *Theor. Chim. Acta* **1990**, *77*, 123.
(29) Deglmann, P.; Furche, F. *J. Chem. Phys.* **2002**, *117*, 9535.
(30) Deglmann, P.; Furche, F.; Ahlrichs, R. *Chem. Phys. Lett.* **2002**, *362*, 511.
(31) Petersilka, M.; Gossmann, U. J.; Gross, E. K. U. *Phys. Rev. Lett.* **1996**, *76*, 1212.
(32) Hirata, S.; Head-Gordon, M. *Chem. Phys. Lett.* **1999**, *314*, 291.
(33) Shao, Y. H.; Head-Gordon, M.; Krylov, A. I. *J. Chem. Phys.* **2003**, *118*, 4807.
(34) Krylov, A. I. *Acc. Chem. Res.* **2006**, *39*, 83.
(35) Krylov, A. I. *Annu. Rev. Phys. Chem.* **2008**, *59*, 433.
(36) Shao, Y.; Molnar, L. F.; Jung, Y.; Kussmann, J.; Ochsenfeld, C.; Brown, S. T.; Gilbert, A. T. B.; Slipchenko, L. V.; Levchenko, S. V.; O'Neill, D. P.; DiStasio, R. A.; Lochan, R. C.; Wang, T.; Beran, G. J. O.; Besley, N. A.; Herbert, J. M.; Lin, C. Y.; Van Voorhis, T.; Chien, S. H.; Sodt, A.; Steele, R. P.; Rassolov, V. A.; Maslen, P. E.; Korambath, P. P.; Adamson, R. D.; Austin, B.; Baker, J.; Byrd, E. F. C.; Dachsel, H.; Doerksen, R. J.; Dreuw, A.; Dunietz, B. D.; Dutoi, A. D.; Furlani, T. R.; Gwaltney, S. R.; Heyden, A.; Hirata, S.; Hsu, C. P.; Kedziora, G.; Khalliulin, R. Z.; Klunzinger, P.; Lee, A. M.; Lee, M. S.; Liang, W.; Lotan, I.; Nair, N.; Peters, B.; Proynov, E. I.; Pieniazek, P. A.; Rhee, Y. M.; Ritchie, J.; Rosta, E.; Sherrill, C. D.; Simmonett, A. C.; Subotnik, J. E.; Woodcock, H. L.; Zhang, W.; Bell, A. T.; Chakraborty, A. K.; Chipman, D. M.; Keil, F. J.; Warshel, A.; Hehre, W. J.; Schaefer, H. F.; Kong, J.; Krylov, A. I.; Gill, P. M. W.; Head-Gordon, M. *Phys. Chem. Chem. Phys.* **2006**, *8*, 3172.
(37) Adamo, C.; Barone, V. *J. Chem. Phys.* **1999**, *110*, 6158.
(38) Hay, P. J.; Wadt, W. R. *J. Chem. Phys.* **1985**, *82*, 299.
(39) Hurley, M. M.; Pacios, L. F.; Christiansen, P. A.; Ross, R. B.; Ermler, W. C. *J. Chem. Phys.* **1986**, *84*, 6840.
(40) Ross, R. B.; Powers, J. M.; Atashroo, T.; Ermler, W. C.; Lajohn, L. A.; Christiansen, P. A. *J. Chem. Phys.* **1990**, *93*, 6654.
(41) Basch, H.; Gray, H. B. *Inorg. Chem.* **1967**, *6*, 365.
(42) Jean, Y. *Molecular Orbitals of Transition Metal Complexes*; Oxford University Press Inc.: New York, 2005.
(43) Marcum, J. C.; Kaufman, S. H.; Weber, J. M. *J. Phys. Chem. A* **2011**, *115*, 3006.